Asian Research Journal of Mathematics

Volume 19, Issue 10, Page 75-95, 2023; Article no.ARJOM.105036
ISSN: 2456-477X

Analytical Solution of Hyperbolic Tangent Fluid's Peristaltic Flow in an Inclined Channel: Hall Effect's Impact

N. Maheshbabu [a*] and S. Rama Mohan [b]

[a] Department of Mathematics, Dr. S.R.K. Govt. Arts College, Yanam-533464. U.T. of Puducherry, India.
[b] Department of Mathematics, PACE Institute of Technology & Sciences (Autonomous), Ongole 523272, A.P., India.

Authors' contributions

This work was carried out in collaboration between both authors. Throughout the whole process of writing this research paper authors NM and SRM worked together in order to prepare it to the highest possible standard. Both authors read and approved the final manuscript.

Article Information

DOI: 10.9734/ARJOM/2023/v19i10730

Open Peer Review History:
This journal follows the Advanced Open Peer Review policy. Identity of the Reviewers, Editor(s) and additional Reviewers, peer review comments, different versions of the manuscript, comments of the editors, etc are available here: https://www.sdiarticle5.com/review-history/105036

Original Research Article

Received: 12/06/2023
Accepted: 16/08/2023
Published: 22/08/2023

Abstract

Aim: In our study, we investigated, based on the premise of a long wavelength, how Hall's theory affected the peristaltic pumping of a fluid with a hyperbolic tangent within an inclined planar channel, and how both affected each other.
Study Design: Abstract, introduction, Statement, Analytical Solution, Results and Discussion, and conclusion.
Methodology: The intra-uterine fluid motion with tiny particles in a non-pregnant uterus is one of the many applications of the current physical problem, and this fluid motion condition is crucial for analysing the motion of the embryo in a uterus. Perturbation-oriented numerical research has been carried out in the current study to characterise the properties of velocity and axial pressure gradient in an inclined channel under Hall effect on the peristaltic flow of a Hyperbolic tangent because of these real-world applications. Under low

**Corresponding author: Email: nmahesh@dhtepdy.edu.in;*

Reynolds number and long-wavelength approximations, the current physical model yields the governing two-dimensional coupled nonlinear flow equations. For different values of the physical parameters, a suitable equation for the stream function is derived, and a regular perturbation scheme is used to produce the numerical solutions in terms of pressure rise and velocity. Weissenberg number, power-law index, Hall parameter, Hartmann number, and amplitude ratio relationships are examined in graphs along with their effects on the axial pressure gradient and time-averaged volume flow rate. According to the findings of this study, whereas the axial pressure gradient and time-averaged flow rate in the pumping region enhance with rising values of the Weissenberg, Hartmann, Reynolds, angle of inclination, and amplitude ratio, they diminish with enhances in the power-law index, Hall parameter, and Froude number. Hyperbolic tangent fluid has been discovered to require less pumping than Newtonian fluid.

Keywords: Hall effect; peristaltic flow; incline channel; hyperbolic tangent fluid.

1 Introduction

Peristaltic transport is a form of fluid transportation that involves a gradual wave of area contraction or expansion down the length of a distensible tube transporting fluid. Peristaltic transport frequently occurs in a range of biological systems, such as the oesophagus, intra-urinary fluid circulation, small blood vessel circulation, and the flow of countless distinct glandular ducts. Many theoretical and practical studies have been done to understand peristalsis using quick changes in geometry and realistic assumptions. Many living organisms use peristaltic fluid flow, including the heart-lung machine, trapping phenomena, pumping, dialysis equipment, reflux, food passing through the oesophagus, fluid motion through lymphatic vessels, and cilia movement. These physical processes are studied by considering well-known non-Newtonian fluid flow models. However, in this direction, the hyperbolic tangent fluid flow model is one of the most significant liquid models in the class of non-Newtonian liquids. From the experimental point of view, it is noticed that the tangent hyperbolic flow model assumes the shear thinning behaviour very exactly. Hyperbolic tangent liquids are mostly used in laboratory experiments, R&D industries, medicine, and engineering fields for various purposes. Following are a few examples of hyperbolic tangent fluid in the field of biology and industry: blood, solutions, whipped cream, ketchup, polymers, melts, nail polish and paints. There are significant practical ramifications for the special group of liquids that have a viscosity that is affected by shear stress or flow rate. The majority of non-Newtonian fluids, including polymers, have viscosities that are nonlinearly declining functions of the generalised shear rate. Shear-thinning behaviour is what is meant by this. A hyperbolic tangent fluid is such a substance (Ai and Vafai, [1]). Nadeem and Akram [2] first investigated the tangent hyperbolic fluid model and found that the narrow part of the channel requires a large pressure gradient, also in the narrow part the pressure gradient decreases with the increase in Weissenberg number (We), and channel width (d). Noreen et el. [3] investigated the Effects of slip and induced magnetic field on the peristaltic flow of pseudoplastic fluid. Prakash et el. [4] studied the effects of the peristaltic flow of a third order fluid in the tapered asymmetric channel are analyzed under longwave length and low Reynolds number situations Akbar et al. [5] investigated The peristaltic flow of a magnetohydrodynamic (MHD) Tangent hyperbolic fluid in an inclined asymmetric channel and the impact of various pertinent parameters is plotted and discussed, and the most interesting mechanism of peristalsis is trapping, which is also taken into account by drawing a stream of all the physical parameters. Prabhakaran et al. [6] the peristaltic transport of a non-Newtonian fourth grade fluid in a channel between two porous beds with suction and injection is investigated. Eldabe et al. [7] explored the influence of hall, heat, and mass transfer on the peristaltic flow of MHD third order fluid under long-wavelength and low Reynolds number approximation. Abbas et al. [8] Three dimensional peristaltic flow of hyperbolic tangent fluid in a non-uniform channel has been investigated and found that the magnitude of the velocity is maximum in the canter of the channel whereas it is minimum near the walls. Saravana et al. [9] Heat and mass transfer are used to investigate the effects of elastic wall properties on the peristaltic transport of a conducting hyperbolic tangent fluid in a non-uniform channel. Then, the trapping phenomenon is examined, and it is found that the size of the trapping bolus grows as the power law index of the hyperbolic tangent fluid increases. Subbanarasimhudu and Subba Reddy [10] investigated the effect of Hall on the peristaltic pumping of a hyperbolic tangent fluid in a planar channel under the assumption of long wavelength. By selecting the Weissenberg number We = 0, the power-law index n = 0, and the Hartmann number M = 0, they were able to assess the results for Newtonian fluid. Sucharitha et al. [11] explored the effects of a magnetic field and slip on the convective peristaltic transport of a Bingham fluid in an inclined nonuniform porous channel with flexible walls and observed that the velocity increases with increasing slip parameter values and decreases with decreasing slip parameter values, whereas the temperature

and heat transfer coefficient exhibits the opposite behaviour, with the velocity, temperature, and heat transfer coefficients decreasing as the magnetic and permeability parameters increase. The channel's incline boosts both velocity and temperature. Selvi and Srinivas [12] investigated how elasticity affected the peristaltic movement of Herschel-Bulkley fluid in a tube with a non-uniform cross-section. The findings indicated that the yield stress and fluid behaviour index have a significant impact on the flux variation of Herschel-Bulkley fluid in a non-uniform elastic tube, and An analysis was done on the influence of elastic factors on flow variation.

We know from biochemistry that positive or negatively charged molecules combine to create cells. As a result, the interplay between molecules and their orientation may undergo substantial changes when these magnetic fields are applied to living things. stimulation of the kidney projection region and upper ureter with remote-controlled impulse magnetic field (IMF) was experimentally studied by Li et al. [13] It was found that IMF activates impulse activity of ureteral smooth muscles in 100% of cases. Hayat et al. [14] first investigated the peristaltic transport of an incompressible, electrically conducting Maxwell fluid in a planar channel. Under a zero Reynolds number and long wavelength approximation, the MHD peristaltic flow of a hyperbolic tangent fluid model in a vertical asymmetric channel was investigated.

In order to analyse blood flow, such as using a catheter or drug delivery, magnetic fields are used Akram and Nadeem [15]. Devaki et al. [16] deal with the analytical investigation of the peristaltic motion of ferromagnetic fluids through a vertical slot with mixed convection. Chakradhar et al. [17] The peristaltic transport of a viscous fluid in an exceedingly porous channel with suction and injection by using the Galerkin method studied. Vidya et al. [18] found that the regulating of velocity due to magnetic constants is observed while the thermal determination of particles displays an enhancing tendency. The consequences of Hall as well as slip taking place on the peristaltic stream of a Jeffrey solution through a permeable middling within an inclined 2D strait below the extensive wavelength estimation are explored by Gangavathi et al. [19]. Investigating the rheological characteristics of biological fluids such as saliva, blood, cerebrovascular fluids, inside cells, and interstitial fluids requires an understanding of Ree-Eyring non-Newtonian fluid peristalsis. Ajithkumar et al. [20] explored the cross-diffusive magnetohydrodynamic peristaltic transport of a Ree–Eyring fluid conveying tiny particles through a flexible porous channel under the influence of activation energy.

The current review of the literature showed that the Hall effect's influence on the peristaltic flow of a fluid with a hyperbolic tangent in an inclined channel has not yet been tried. This was accomplished using the long wavelength supposition. Additionally, this paper uses the perturbation strategy to generate semi-numerical solutions in an inclined channel with peristaltic flow of a Hyperbolic tangent. The expressions for the velocity and axial pressure gradient are obtained by using the perturbation technique. The flow patterns are represented in terms of the Weissenberg number, power-law index, Hall parameter, Hartmann number, and amplitude ratio on the axial pressure gradient and time-averaged volume flow rate. The relationships between the Weissenberg number, power-law index, Hall parameter, Hartmann number, and amplitude ratio and how they impact the axial pressure gradient and time-averaged volume flow rate are examined using graphs.

2 Statement

We explore the peristaltic flow of a fluid with a hyperbolic tangent in a symmetric, two-dimensional channel with width 2a in the presence of a magnetic field. The flow is produced by sinusoidal wave trains propagating along the channel walls at a constant speed. The transverse direction of the flow is subjected to a constant magnetic field B_0. The resultant magnetic field

is disregarded due to the perception that the magnetic Reynolds quantity is negligible. Fig. 1. precisely represented the physical characteristics of fluid flow along a hyperbolic tangent. Considering the aforementioned flow hypotheses, the current flow mechanism is defined as follows: [2,5,8,10]

$$Y = \pm H(X,t) = \pm a \pm b\cos\frac{2\pi}{\lambda}(X - ct) \tag{1}$$

where X, Y are the rectangular coordinates, λ is the wavelength, and b is the wave's amplitude. X measured perpendicular to X and parallel to the channel's axis.

In the lab frame (X,Y), the flow is erratic. The boundary form, however, is stationary in a coordinate system moving at the propagation velocity c.

The equation for the conversion of the fixed frame to the wave frame is

$$x = X - ct, y = Y, u = U - c, v = V \tag{2}$$

where the wave and fixed frames' respective velocity components, (u,v) and (U,V), are given.

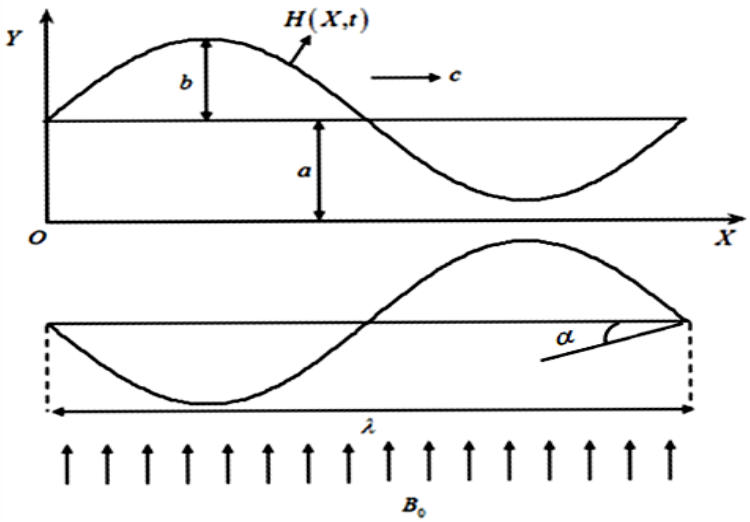

Fig. 1. The channel's physical model [10]

The computation process for switching between the fixed frame to a wave frame is as follows:

A hyperbolic tangent fluid's constitutive equation is [2,5,8,10]

$$\tau = -\left[\eta_\infty + \left(\eta_0 + \eta_\infty\right)\tanh\left(\Gamma\dot{\gamma}\right)^n\right]\dot{\gamma} \tag{3}$$

$\dot{\gamma}$ consists of the following

$$\dot{\gamma} = \sqrt{\frac{1}{2}\sum_i\sum_j \dot{\gamma}_{ij}\dot{\gamma}_{ji}} = \sqrt{\frac{1}{2}\pi} \tag{4}$$

Consequently, equation (3) has the following structure: For $\eta_\infty = 0$ and $\Gamma\dot{\gamma} < 1$,

$$\tau = -\eta_0\left(\Gamma\dot{\gamma}\right)^n\dot{\gamma} = -\eta_0\left(1+\Gamma\dot{\gamma}-1\right)^n\dot{\gamma} = -\eta_0\left(1+n\left[\Gamma\dot{\gamma}-1\right]\right)\dot{\gamma} \tag{5}$$

For $\Gamma = 0$ and $n = 0$, the aforementioned model is reduced to Newtonian.

In the wave frame of reference, the equations regulating the flow are: [2,5,8,10]

$$\frac{\partial u}{\partial x} + \frac{\partial v}{\partial y} = 0 \tag{6}$$

$$\left(u\frac{\partial u}{\partial x}+v\frac{\partial u}{\partial y}\right)\rho=-(\frac{\partial p}{\partial x}+\frac{\partial \tau_{xx}}{\partial x}+\frac{\partial \tau_{yx}}{\partial y})+\frac{\sigma B_0^2}{1+m^2}\left(mv-u-c\right)+\rho g\sin\alpha \tag{7}$$

$$\left(u\frac{\partial v}{\partial x}+v\frac{\partial u}{\partial y}\right)\rho=-(\frac{\partial p}{\partial y}+\frac{\partial \tau_{xy}}{\partial x}+\frac{\partial \tau_{yy}}{\partial y})-\frac{\sigma B_0^2}{1+m^2}\left(v+m\left(u+c\right)\right)-\rho g\cos\alpha \tag{8}$$

where B_0 = the intensity of the magnetic field, ρ = density, σ = electrical conductivity, and m = Hall parameter.

Dimensional boundary conditions include the following:

at $y=H$, $u=-c$ (9)

at $y=0$, $\frac{\partial u}{\partial y}=0$ (10)

including the non-dimensional variables mentioned: [2,5,8,10]

$$\bar{x}=\frac{x}{\lambda},\ \bar{y}=\frac{y}{a},\ \bar{u}=\frac{u}{c},\ \bar{v}=\frac{v}{c\delta},\ \delta=\frac{a}{\lambda},\ \bar{p}=\frac{pa^2}{\eta_0 c\lambda},\phi=\frac{b}{a}$$

$$h=\frac{H}{a},\ \bar{t}=\frac{ct}{\lambda},\ \bar{\tau}_{xx}=\frac{\lambda}{\eta_0 c}\tau_{xx},\ \bar{\tau}_{xy}=\frac{a}{\eta_0 c}\tau_{xy},\ \bar{\tau}_{yy}=\frac{a}{\eta_0 c}\tau_{yy},$$

$$\mathrm{Re}=\frac{\rho ac}{\eta_0},\ We=\frac{\Gamma c}{a},\ \bar{\dot{\gamma}}=\frac{\dot{\gamma}a}{c},\ \bar{q}=\frac{q}{ac},Fr=\frac{c^2}{ag} \tag{11}$$

into the equations (6) - (8), following the bars being dropped, reduce to

$$\frac{\partial u}{\partial x}+\frac{\partial v}{\partial y}=0 \tag{12}$$

$$\mathrm{Re}\,\delta\left(u\frac{\partial u}{\partial x}+v\frac{\partial u}{\partial y}\right)=-\frac{\partial p}{\partial x}-\delta^2\frac{\partial \tau_{xx}}{\partial x}-\frac{\partial \tau_{xy}}{\partial y}+\frac{M^2}{1+m^2}\left(m\delta v-\left(u+1\right)\right)+\frac{\mathrm{Re}}{Fr}\sin\alpha \tag{13}$$

$$\mathrm{Re}\,\delta^3\left(u\frac{\partial v}{\partial x}+v\frac{\partial v}{\partial y}\right)=-\frac{\partial p}{\partial y}-\delta^2\frac{\partial \tau_{xy}}{\partial y}-\delta\frac{\partial \tau_{yy}}{\partial y}-\frac{\delta M^2}{1+m^2}\left(m\left(u+1\right)+\delta v\right)-\frac{\mathrm{Re}}{Fr}\delta\cos\alpha \tag{14}$$

Were, $\tau_{xx}=-2\left[1+n\left(We\dot{\gamma}-1\right)\right]\frac{\partial u}{\partial x}$, $\tau_{xy}=-\left[1+n\left(We\dot{\gamma}-1\right)\right]\left(\frac{\partial u}{\partial y}+\delta^2\frac{\partial v}{\partial x}\right)$,

$$\tau_{yy}=-2\delta\left[1+n\left(We\dot{\gamma}-1\right)\right]\frac{\partial v}{\partial y},\ \dot{\gamma}=\left[2\delta^2\left(\frac{\partial u}{\partial x}\right)^2+\left(\frac{\partial u}{\partial y}+\delta^2\frac{\partial v}{\partial x}\right)^2+2\delta^2\left(\frac{\partial v}{\partial y}\right)^2\right]^{\frac{1}{2}}$$

And Hartmann number $M = aB_0\sqrt{\frac{\sigma}{\eta_0}}$.

The equations (13) and (14) under the lubrication approach become simpler by ignoring the terms of order δ and Re.

$$\frac{\partial p}{\partial x} = \frac{\partial}{\partial y}\left\{\left[1+n\left(We\frac{\partial u}{\partial y}-1\right)\right]\frac{\partial u}{\partial y}\right\} - \frac{M^2}{1+m^2}(u+1) + \frac{\mathrm{Re}}{Fr}\sin\alpha \tag{15}$$

$$\frac{\partial p}{\partial y} = 0 \tag{16}$$

Equations (15) and (16) allow us to derive

$$\frac{dp}{dx} = (1-n)\frac{\partial^2 u}{\partial y^2} + nWe\frac{\partial}{\partial y}\left[\left(\frac{\partial u}{\partial y}\right)^2\right] - \frac{M^2}{1+m^2}(u+1) + \frac{\mathrm{Re}}{Fr}\sin\alpha \tag{17}$$

In the wave frame, the equivalent non-dimensional boundary conditions are provided by

$$u = -1 \qquad \text{at} \qquad y = h = 1+\phi\cos 2\pi x \tag{18}$$

$$\frac{\partial u}{\partial y} = 0 \qquad \text{at} \qquad y = 0 \tag{19}$$

In a wave frame of reference, the volume flow rate is calculated using the simple formula

$$q = \int_0^h u dy \tag{20}$$

The laboratory's instantaneous flow frame $Q(X,t)$ is

$$Q(X,t) = \int_0^h U dY = \int_0^h (u+1)dy = q+h \tag{21}$$

For the time-averaged volume flow rate of the peristaltic wave over a period T, expressed as:

$$\overline{Q} = \frac{1}{T}\int_0^T Q dt = q+1 \tag{22}$$

3 Analytical Solution

Since equation (17) is a non-linear differential equation, it is not possible to obtain a closed-form solution. Therefore, we employ regular perturbation to find the solution.

For the perturbation solution, we expand $u, \frac{dp}{dx}$, q as follows

$$u = u_0 + We\, u_1 + O\left(We^2\right) \tag{23}$$

$$\frac{dp}{dx} = \frac{dp_0}{dx} + We\frac{dp_1}{dx} + O\left(We^2\right) \tag{24}$$

$$q = q_0 + We\, q_1 + O\left(We^2\right) \tag{25}$$

Substituting these equations into the equations (17) - (19), we obtain

3.1 System of order We^0

$$\frac{dp_0}{dx} = (1-n)\frac{\partial^2 u_0}{\partial y^2} - \frac{M^2}{1+m^2}(u_0+1) + \frac{\mathrm{Re}}{Fr}\sin\alpha \tag{26}$$

and the respective boundary conditions are

$$u_0 = -1 \qquad \text{at} \qquad y = h \tag{27}$$

$$\frac{\partial u_0}{\partial y} = 0 \qquad \text{at} \qquad y = 0 \tag{28}$$

3.2 System of order We^1

$$\frac{dp_1}{dx} = (1-n)\frac{\partial^2 u_1}{\partial y^2} + n\frac{\partial}{\partial y}\left[\left(\frac{\partial u_o}{\partial y}\right)^2\right] - \frac{M^2}{1+m^2}u_1 \tag{29}$$

and the respective boundary conditions are

$$u_1 = 0 \qquad \text{at} \qquad y = h \tag{30}$$

$$\frac{\partial u_1}{\partial y} = 0 \qquad \text{at} \qquad y = 0 \tag{31}$$

3.3 Solution for the system of order We^0

To solve equation (26), we use the boundary conditions (27) and (28).

$$u_0 = \frac{1}{\beta^2(1-n)}\left(\frac{dp_0}{dx} - \frac{\mathrm{Re}}{Fr}\sin\alpha\right)\left[\frac{\cosh\beta y}{\cosh\beta h} - 1\right] - 1 \tag{32}$$

where $\beta = M / \sqrt{(1-n)(1+m^2)}$.

The volume flow rate q_0 is given by

$$q_0 = \frac{1}{\beta^3(1-n)}\left(\frac{dp_0}{dx} - \frac{\mathrm{Re}}{Fr}\sin\alpha\right)\left[\frac{\sinh\beta h - \beta h\cosh\beta h}{\cosh\beta h}\right] - h \tag{33}$$

From equation (3.11), we have

$$\frac{dp_0}{dx} = \frac{(q_0+h)\beta^3(1-n)\cosh\beta h}{\left[\sinh\beta h - \beta h\cosh\beta h\right]} + \frac{\mathrm{Re}}{Fr}\sin\alpha \tag{34}$$

3.4 Solution for the system of order We^1

Equation (32) is substituted for equation (29), equation (29) is solved, equation (29) is used to apply the boundary conditions (30) and (31), and the result is

$$u_1 = \frac{1}{\beta^2(1-n)}\frac{dp_1}{dx}\left[\frac{\cosh\beta y}{\cosh\beta h} - 1\right] + \frac{n}{3}\frac{\left(\frac{dp_0}{dx} - \frac{\mathrm{Re}}{Fr}\sin\alpha\right)^2}{\left[\beta(1-n)\cosh\beta h\right]^3}\left[\begin{matrix}(\sinh 2\beta h - 2\sinh\beta h)\cosh\beta y \\ +(2\sinh\beta y - \sinh 2\beta y)\cosh\beta h\end{matrix}\right] \tag{35}$$

The volume flow rate q_1 is given by

$$q_1 = \frac{1}{\beta^3(1-n)}\frac{dp_1}{dx}\left[\frac{\sinh\beta h - \beta h\cosh\beta h}{\cosh\beta h}\right] + A_1\left(\frac{dp_0}{dx} - \frac{\mathrm{Re}}{Fr}\sin\alpha\right)^2 \tag{36}$$

where $A_1 = n\left(\frac{4 - 3\cosh\beta h + 2\sinh 2\beta h\sinh\beta h - \cosh\beta h\cosh 2\beta h}{6\beta^4(1-n)^3\cosh^3\beta h}\right)$.

From equations (36) and (34), we have

$$\frac{dp_1}{dx} = \frac{q_1\beta^3(1-n)\cosh\beta h}{\left[\sinh\beta h - \beta h\cosh\beta h\right]} - A_2\left(\frac{dp_0}{dx} - \frac{\mathrm{Re}}{Fr}\sin\alpha\right)^2 \tag{37}$$

where $A_2 = n\left(\frac{4 - 3\cosh\beta h + 2\sinh 2\beta h\sinh\beta h - \cosh\beta h\cosh 2\beta h}{6\beta(1-n)^2\cosh^2\beta h(\sinh\beta h - \beta h\cosh\beta h)}\right)$.

Equations (24) are changed by substituting equations (34) and (37), using

relation $q_o = q - Weq_1$ and neglecting terms greater than $O(We)$, we get

$$\frac{dp}{dx} = \frac{(q+h)\beta^3(1-n)\cosh\beta h}{\left[\sinh\beta h - \beta h\cosh\beta h\right]} - \frac{WeA_3\beta^5}{6}\frac{(q+h)^2}{(\sinh\beta h - \beta h\cosh\beta h)^3} + \frac{\mathrm{Re}}{Fr}\sin\alpha \tag{38}$$

where $A_3 = 4 - 3\cosh\beta h + 2\sinh 2\beta h \sinh\beta h - \cosh\beta h \cosh 2\beta h$.

As follows is the definition of the dimensionless pressure increase per wave frame wavelength:

$$\Delta p = \int_0^1 \frac{dp}{dx} dx \tag{39}$$

It is feasible to confirm and establish the veracity of the current peristaltic flow model by comparing the current solutions to the prior outcomes of Subbanarasimhudu and Subba Reddy (12) with $\alpha \to 0$.

4 Results and Discussion

Fig. 2. describes the variation of the axial pressure gradient ($\frac{dp}{dx}$) with Weissenberg number (We) for $n = 0.5$, $m = 0.3$, $M = 1$, $\phi = 0.5$, $\mathrm{Re} = 5$, $\alpha = \frac{\pi}{6}$, $Fr = 2$ and $\overline{Q} = -1$. This is what is noticed, Increasing $\frac{dp}{dx}$ causes We to increase

The relationship between the power-law index (n) and the axial pressure gradient ($\frac{dp}{dx}$) for $We = 0.01$, $m = 0.3$, $M = 1$, $\phi = 0.5$, $\mathrm{Re} = 5$, $\alpha = \frac{\pi}{6}$, $Fr = 2$ and $\overline{Q} = -1$ is shown in Fig. 3. It has been noted that, With n , $\frac{dp}{dx}$ falls off.

Fig. 4 displays the variation of the axial pressure gradient ($\frac{dp}{dx}$) with the Hall parameter (m) for $n = 0.5$, $We = 0.01$, $M = 1$, $\phi = 0.5$, $\mathrm{Re} = 5$, $\alpha = \frac{\pi}{6}$, $Fr = 2$ and $\overline{Q} = -1$. The finding is, as m increases, $\frac{dp}{dx}$ lowers.

Changes in the axial pressure gradient ($\frac{dp}{dx}$) with Hartmann number (M) for $n = 0.5$, $m = 0.3$, $We = 0.01$, $\phi = 0.5$, $\mathrm{Re} = 5$, $\alpha = \frac{\pi}{6}$, $Fr = 2$ and $\overline{Q} = -1$ is seen in Fig 5. It has been observed that raising M raises $\frac{dp}{dx}$.

Fig. 6. illustrates the variation of the axial pressure gradient ($\frac{dp}{dx}$) with Reynolds number (Re) for $n = 0.5$, $We = 0.01$, $M = 1$, $\phi = 0.5$, $m = 0.3$, $\alpha = \frac{\pi}{6}$, $Fr = 2$ and $\overline{Q} = -1$. The finding when rises Re, $\frac{dp}{dx}$ rises as well.

The relationship between the Froude number (Fr) and the axial pressure gradient ($\frac{dp}{dx}$) for $n=0.5$, $m=0.3$, $We=0.01$, $\phi=0.5$, $\mathrm{Re}=5$, $\alpha=\frac{\pi}{6}$, $M=1$ and $\overline{Q}=-1$ is displayed in Fig. 7. It has been found that raising Fr results in a decrease in $\frac{dp}{dx}$.

Fig. 8. demonstrates the variation of the axial pressure gradient ($\frac{dp}{dx}$) with inclination angle (α) for $n=0.5$, $m=0.3$, $M=1$, $We=0.01$, $\mathrm{Re}=5$, $\phi=0.5$, $Fr=2$ and $\overline{Q}=-1$. It is discovered that as α grows, so does $\frac{dp}{dx}$.

The relationship between the amplitude ratio (ϕ) and the axial pressure gradient ($\frac{dp}{dx}$) for $n=0.5$, $m=0.3$, $M=1$, $We=0.01$, $\mathrm{Re}=5$, $\alpha=\frac{\pi}{6}$, $Fr=2$ and $\overline{Q}=-1$ is depicted in Fig. 9. As the amplitude ratio ϕ increases, it is observed that the axial pressure gradient $\frac{dp}{dx}$ also increases.

Fig. 10 shows how the pressure rise Δp changes depending on the Weissenberg number (We) and the time-averaged volume flow rate ($\overline{Q}$) with $n=0.5$, $m=0.3$, $M=1$, $\mathrm{Re}=5$, $\alpha=\frac{\pi}{6}$, $Fr=2$ and $\phi=0.5$. In regions of pumping $(\Delta p>0)$, free pumping $(\Delta p=0)$, and co-pumping $(\Delta p<0)$, it is seen that $\overline{Q}$ rises with rising We.

Comparison of the pressure rise Δp variation with time-averaged flow rates ($\overline{Q}$) for various power-law index (n) values with $We=0.01$, $m=0.3$, $M=1$, $\mathrm{Re}=5$, $\alpha=\frac{\pi}{6}$, $Fr=2$ and $\phi=0.5$ is portrayed in Fig. 11. It is noted that, $\overline{Q}$ decreases with an increase n in both the pumping and free pumping regions, while it increases with an increase n in the co pumping region. Notably, $\overline{Q}$ reduces with an increase n in the pumping and free pumping zones, whereas it increases with an increase in n the co-pumping region.

Based on the time-averaged flow rate ($\overline{Q}$) and different Hall parameter (m) values, Fig. 12. shows how pressure rise Δp changes with $n=0.5$, $We=0.01$, $M=1$, $\mathrm{Re}=5$, $\alpha=\frac{\pi}{6}$, $Fr=2$ and $\phi=0.5$. In the pumping region, $\overline{Q}$ is observed to decrease with an increase m, whereas, in the regions of free pumping and co-pumping, it increases with an increase m.

with $n=0.5$, $m=0.3$, $We=0.01$, $\mathrm{Re}=5$, $\alpha=\frac{\pi}{6}$, $Fr=2$ and $\phi=0.5$ The variation of the pressure rise Δp with the time-averaged flow rate ($\overline{Q}$) for different values of Hartmann number (M) is shown in Fig.

13. As M increases in the pumping region, the time-averaged flow rate $\overline{Q}$ is observed to grow, while in the free pumping and co pumping regions, it decreases.

As depicted in Fig. 14, the pressure rise Δp varies with Reynolds number (Re) and the time-averaged flow rate $(\overline{Q})$ for different values of $n=0.5$, $We=0.01$, $M=1$, $m=0.3$, $\alpha=\frac{\pi}{6}$, $Fr=2$ and $\phi=0.5$. In all pumping, free pumping, and co-pumping areas, it is discovered that Q rises as R rises.

For different Froude number Fr values with $n=0.5$, $m=0.3$, $We=0.01$, $\mathrm{Re}=5$, $\alpha=\frac{\pi}{6}$, $M=1$ and $\phi=0.5$, the relationship between the pressure rise Δp and the time-averaged flow rate $(\overline{Q})$ is demonstrated in Fig. 15. In all regions of pumping, free pumping, and co-pumping, it is seen that $\overline{Q}$ falls off as Fr rises.

For varied values of inclination angle (α), with $n=0.5$, $We=0.01$, $M=1$, $m=0.3$, $\mathrm{Re}=5$, $Fr=2$ and $\phi=0.5$, Fig. 16 illustrates the fluctuation of the pressure rise Δp with the time-averaged flow rate $(\overline{Q})$. It has been found that $\overline{Q}$ rises along with rising α in all regions of pumping, free pumping, and co-pumping.

Fig. 17. depicts the amplitude ratio (ϕ), which varies for different values with $n=0.5$, $m=0.3$, $M=1$, $\mathrm{Re}=5$, $\alpha=\frac{\pi}{6}$, $Fr=2$ and $We=0.01$, for the pressure rise Δp and the time-averaged flow rate $(\overline{Q})$. In the regions of pumping and free pumping, $\overline{Q}$ is seen to increase as ϕ increases, whereas in the region of co-pumping for chosen $\Delta p(<0)$, $\overline{Q}$ is seen to decrease as ϕ increases.

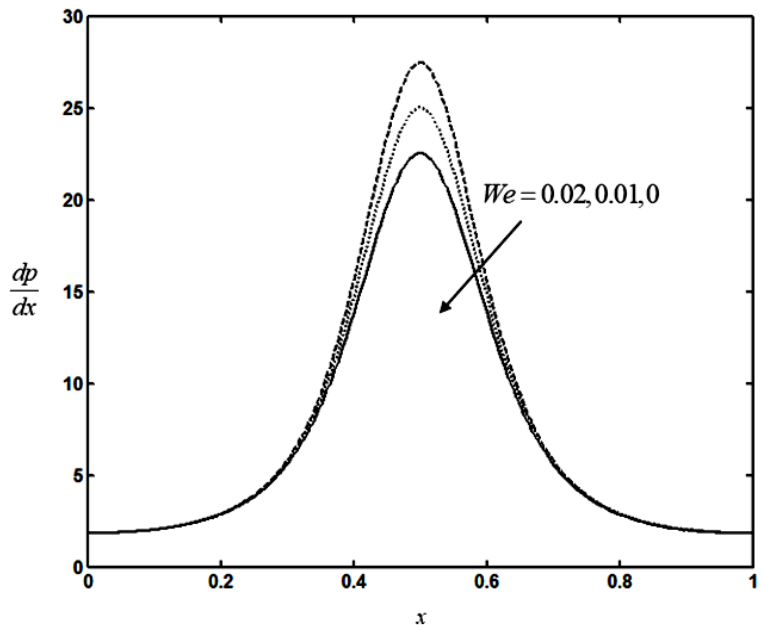

Fig. 2. The variation of the axial pressure gradient $\frac{dp}{dx}$ with We for $n=0.5, m=0.3$, $M=1$, $\phi=0.5, \mathrm{Re}=5$, $\alpha=\frac{\pi}{6}$, $Fr=2$ and $\overline{Q}=-1$

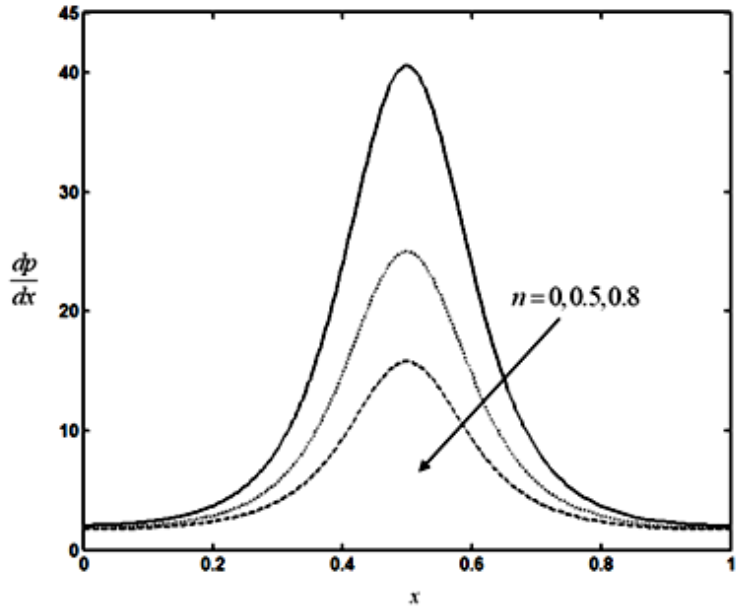

Fig. 3. The variation of the axial pressure gradient $\frac{dp}{dx}$ with n for, $m=0.3, M=1, \phi=0.5,$ $\mathrm{Re}=5, \alpha=\frac{\pi}{6}, Fr=2$ and $\overline{Q}=-1$.

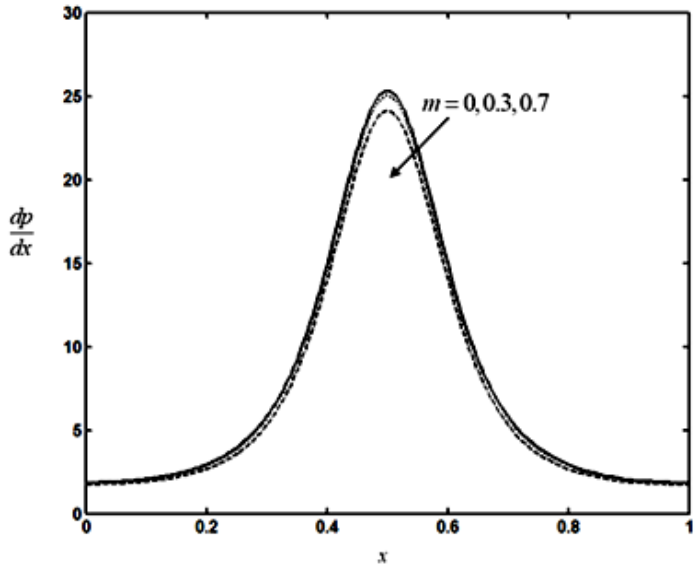

Fig. 4. The variation of the axial pressure gradient $\frac{dp}{dx}$ with m for $n=0.5, We=0.01, M=1,$ $\phi=0.5, \mathrm{Re}=5, \alpha=\frac{\pi}{6}, Fr=2$ and $\overline{Q}=-1$

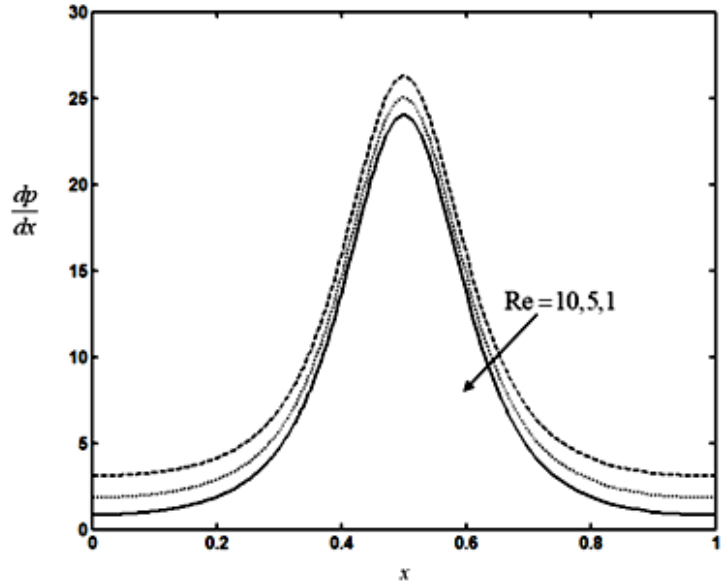

Fig. 5. The variation of the axial pressure gradient $\frac{dp}{dx}$ with M for $n=0.5$, $m=0.3$, $We=0.01$, $\phi=0.5$, $\mathrm{Re}=5$, $\alpha=\frac{\pi}{6}$, $Fr=2$

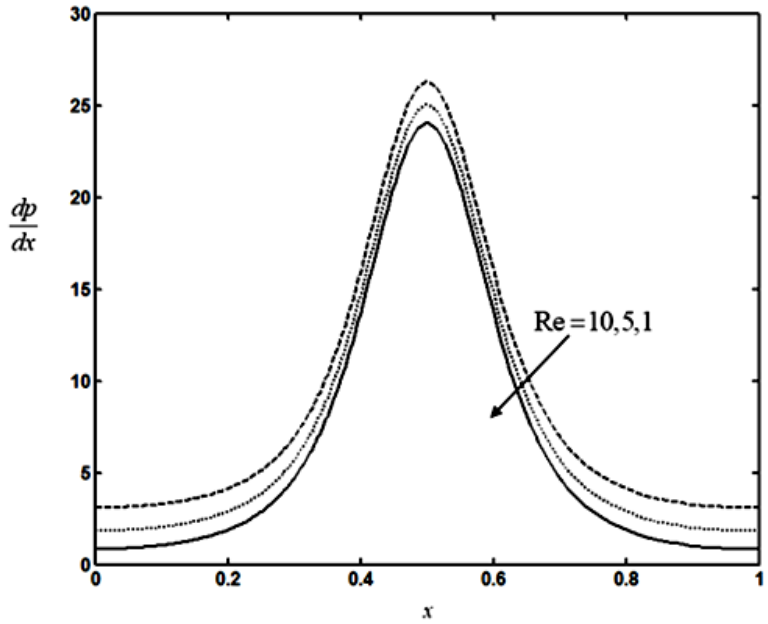

Fig. 6. The variation of the axial pressure gradient $\frac{dp}{dx}$ with Re for $n=0.5$, $m=0.3$, $We=0.01$, $\phi=0.5$, $M=1$, $\alpha=\frac{\pi}{6}$, $Fr=2$.

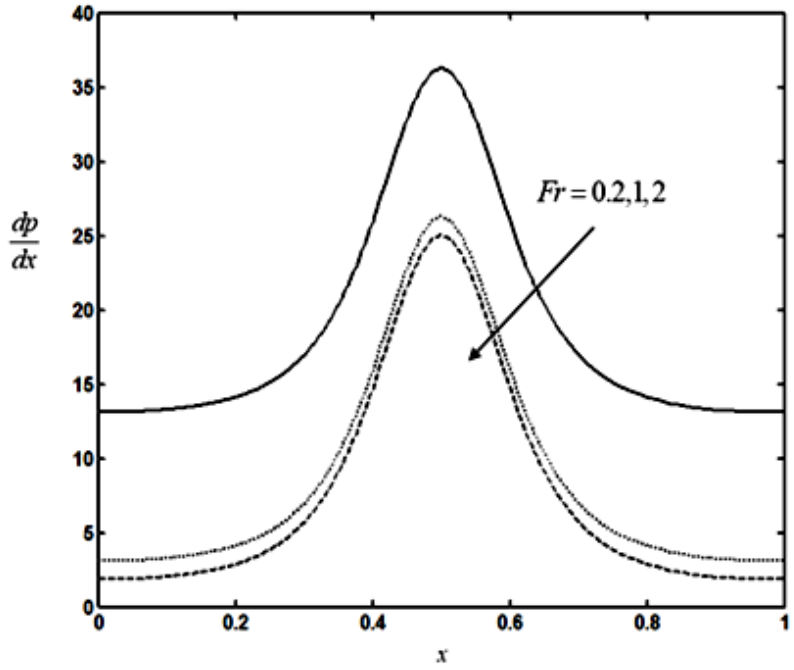

Fig. 7. The variation of the axial pressure gradient $\frac{dp}{dx}$ with Fr for $n = 0.5$, $m = 0.3$, $We = 0.01$, $\mathrm{Re} = 5$, $\alpha = \frac{\pi}{6}$, $\phi = 0.5$ and $\overline{Q} = -1$.

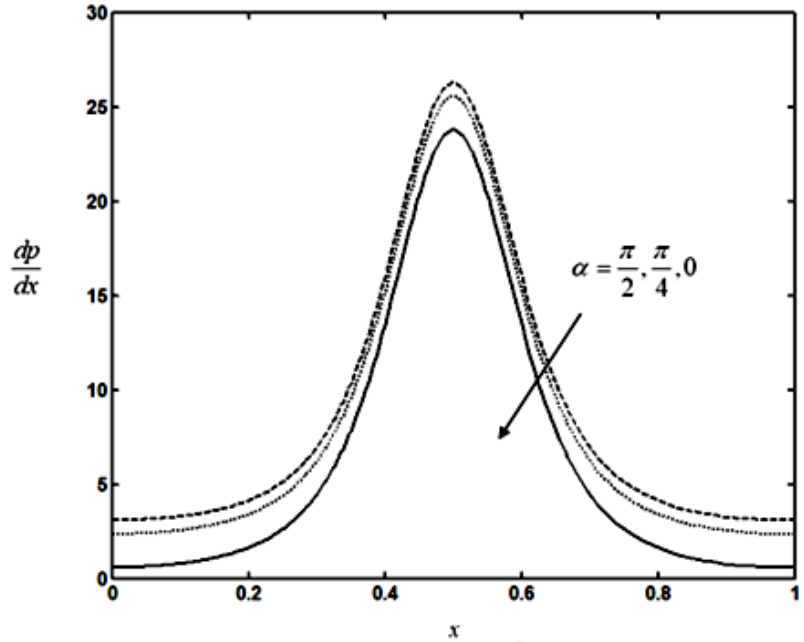

Fig. 8. The variation of the axial pressure gradient $\frac{dp}{dx}$ with α for $n = 0.5$, $m = 0.3$, $We = 0.01$, $\phi = 0.5$, $\mathrm{Re} = 5$, $Fr = 2$ and $\overline{Q} = -1$.

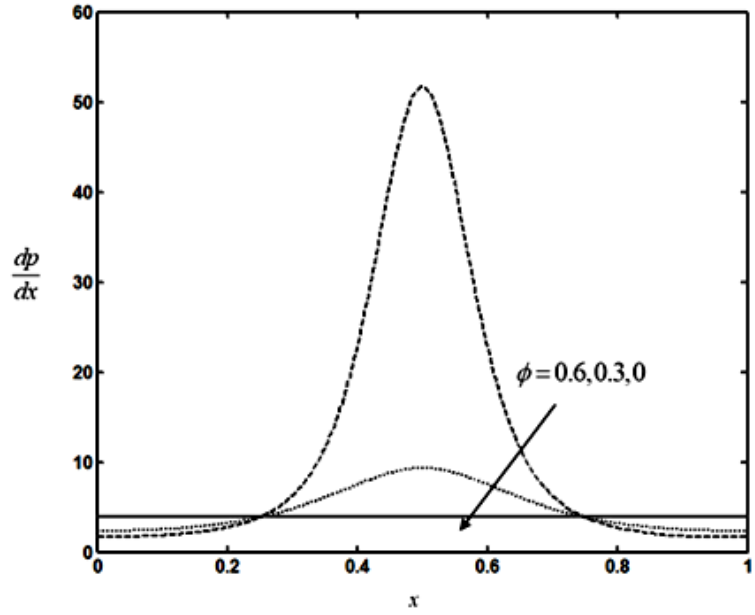

Fig. 9. The variation of the axial pressure gradient $\frac{dp}{dx}$ with ϕ for $n = 0.5$, $m = 0.3$, $M = 1$, $We = 0.01$, $\mathrm{Re} = 5$, $\alpha = \frac{\pi}{6}$, $Fr = 2$ and $\overline{Q} = -1$.

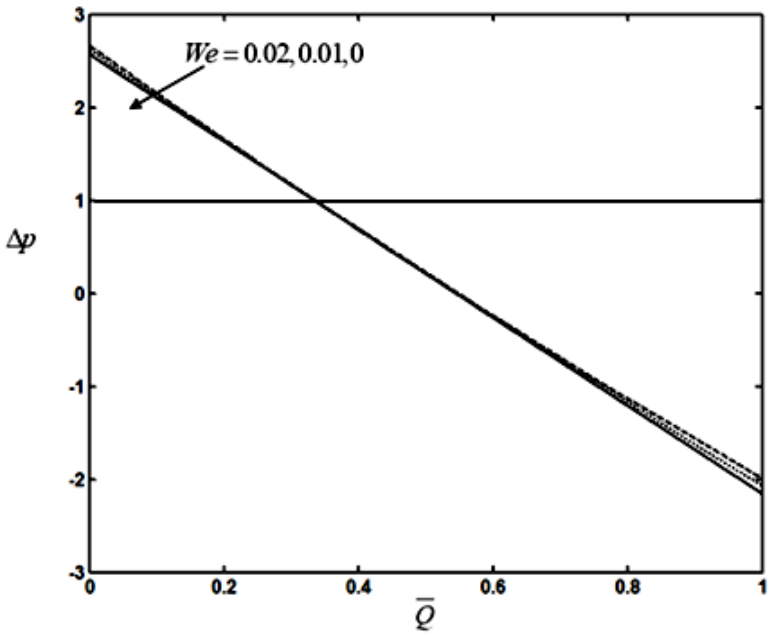

Fig. 10. The variation of the pressure rise Δp with $\overline{Q}$ for different values of We with $n = 0.5$, $m = 0.3$, $M = 1$, $\mathrm{Re} = 5$, $\alpha = \frac{\pi}{6}$, $Fr = 2$ and $\phi = 0.5$.

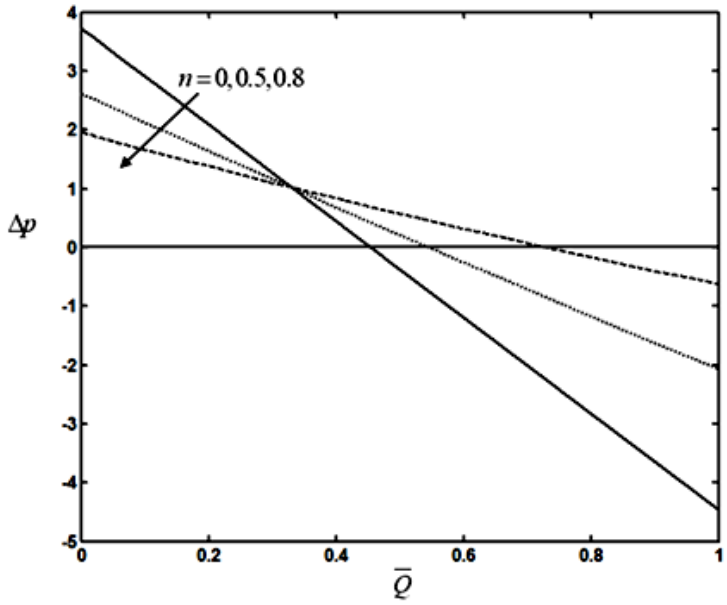

Fig. 11. The variation of the pressure rise Δp with $\bar{Q}$ for different values of n with $We = 0.01$, $m = 0.3$, $M = 1$, $\mathrm{Re} = 5$, $\alpha = \frac{\pi}{6}$, $Fr = 2$ and $\phi = 0.5$.

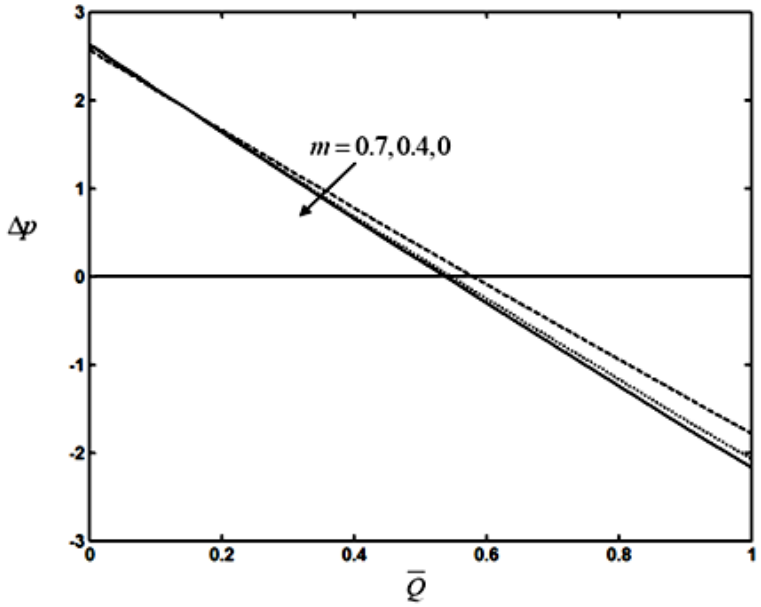

Fig. 12. The variation of the pressure rise Δp with $\bar{Q}$ for different values of m with $n = 0.5$, $We = 0.01$, $M = 1$, $\mathrm{Re} = 5$, $\alpha = \frac{\pi}{6}$, $Fr = 2$ and $\phi = 0.5$.

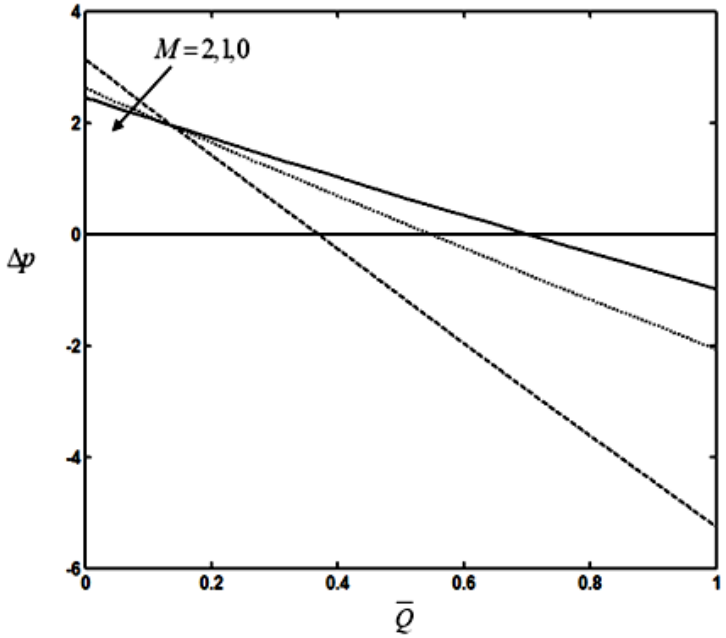

Fig. 13. The variation of the pressure rise Δp with $\bar{Q}$ for different values of M with $n = 0.5$, $m = 0.3$, $We = 0.01$, $\mathrm{Re} = 5$, $\alpha = \frac{\pi}{6}$, $Fr = 2$ and $\phi = 0.5$.

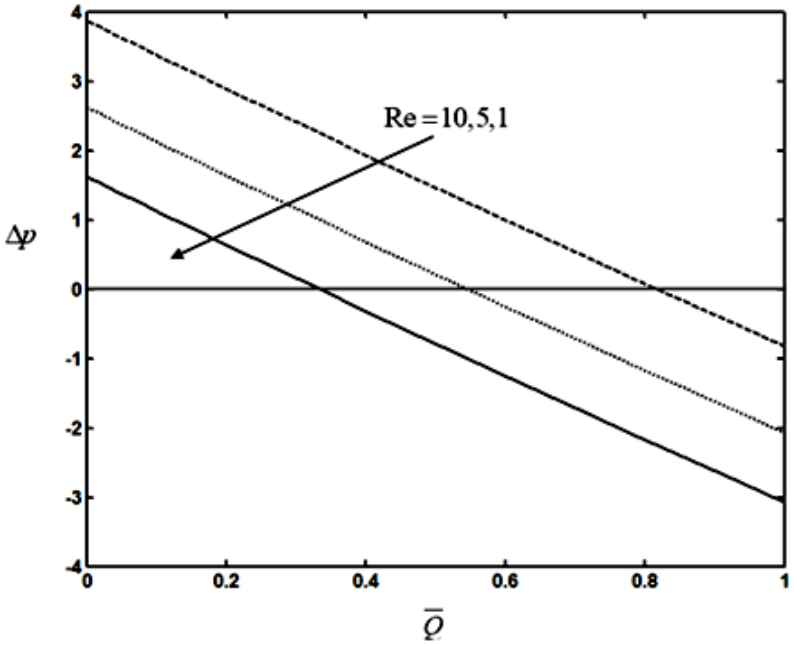

Fig. 14. The variation of the pressure rise Δp with $\bar{Q}$ for different values of Re with $n = 0.5$, $m = 0.3$, $M = 1$, $\phi = 0.5$, $\alpha = \frac{\pi}{6}$, $Fr = 2$ and $We = 0.01$.

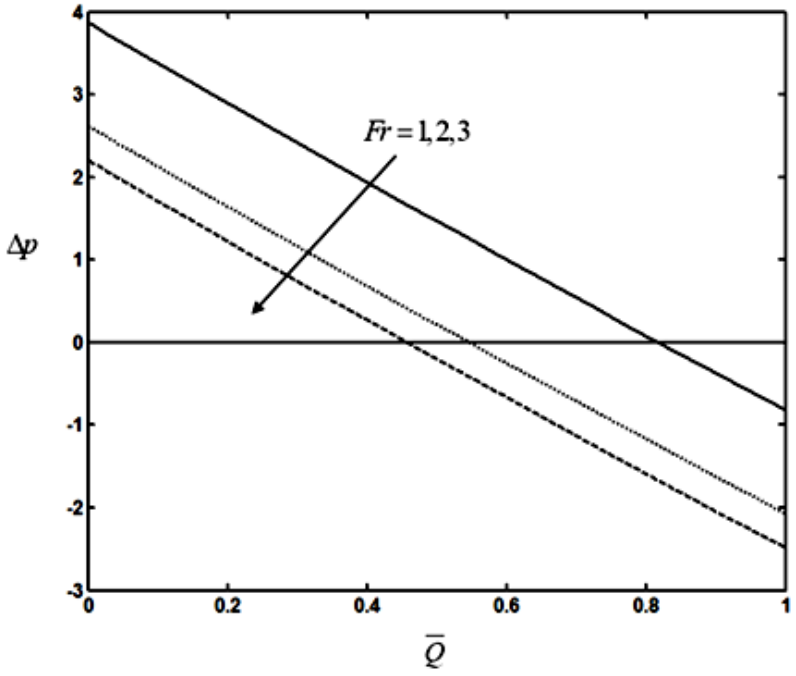

Fig. 15. The variation of the pressure rise Δp with $\bar{Q}$ for different values of Fr with $n = 0.5$, $m = 0.3$, $M = 1$, $\mathrm{Re} = 5$, $\alpha = \frac{\pi}{6}$, $\phi = 0.5$ and $We = 0.01$.

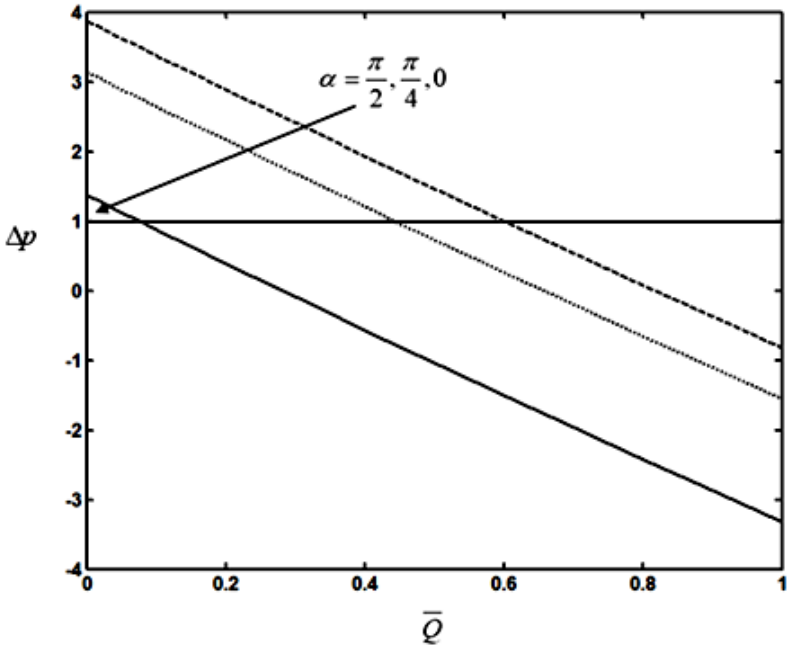

Fig. 16. The variation of the pressure rise Δp with $\bar{Q}$ for different values of α with $n = 0.5$, $m = 0.3$, $M = 1$, $\mathrm{Re} = 5$, $\phi = 0.5$, $Fr = 2$ and $We = 0.01$.

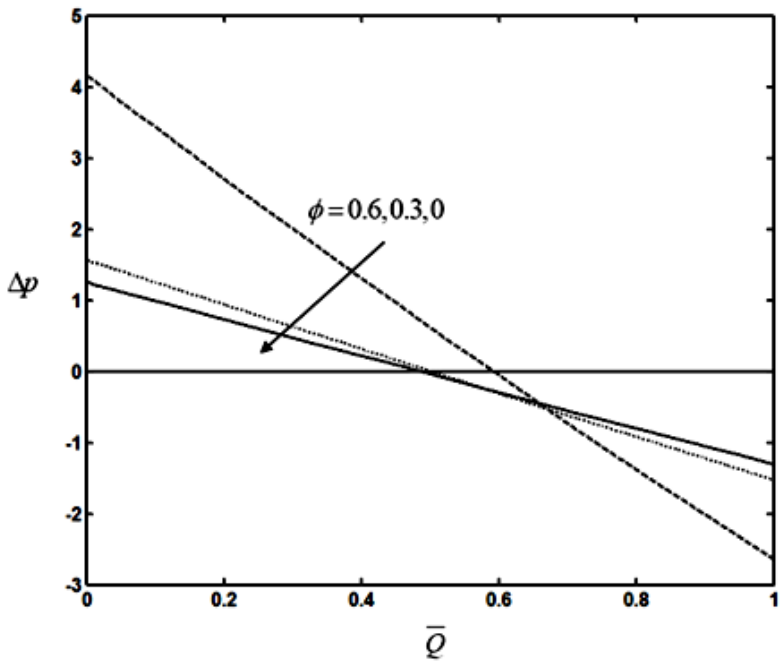

Fig. 17. The variation of the friction force F with $\bar{Q}$ for different values of ϕ with $n = 0.5$, $m = 0.3, \mathrm{Re} = 5$, $\alpha = \frac{\pi}{6}$, $Fr = 2$, $M = 1$ and $We = 0.01$.

5 Conclusions

This study examines the impact of Hall on the peristaltic pumping of a fluid with a hyperbolic tangent in an inclined planar channel under the long wavelength assumption. Using the perturbation technique, the expressions for the velocity and axial pressure gradient are obtained.

It is found that the axial pressure gradient and time-averaged flow rate in the pumping region increase with increasing the Weissenberg number We, the Hartmann number M, the Reynolds number Re, the angle of inclination α, and the amplitude ratio ϕ, while they decrease with increasing power-law index n, Hall parameter m and the Froude number Fr.

When compared to Newtonian fluid, it has been found that hyperbolic tangent fluid requires less pumping.

By way of conclusion, we can say that this work will be very beneficial for authors who wish to continue it in the future by incorporating various physical aspects, slip circumstances, convective boundary circumstances, fluctuating fluid characteristics, etc.

Competing Interests

Authors have declared that no competing interests exist.

References

[1] Ai L, Vafai K. An investigation of Stokes' second problem for non-Newtonian fluids, Numerical Heat Transfer, Part A. 2005;47:955–980.

[2] Nadeem S, Akram S. Peristaltic transport of a hyperbolic tangent fluid model in anasymmetric channel, Z. Naturforsch. 2009;64a:559–567.

[3] Hayat, T., Ali, N. and Asghar, S. Hall effects on peristaltic flow of a Maxwell fluid in a porous medium, Physics Letters A, 363(5-6) (2007), 397–403.

[4] Nadeem S, Noreen Sher Akbar. Numerical analysis of peristaltic transport of a tangent hyperbolic fluid in an endoscope. Journal of Aerospace engineering. 2011;24(3):309-317.

[5] Noreen S, Hayat T, Alsaedi A. Study of slip and induced magnetic field on the peristaltic flow of pseudoplastic fluid, International Journal of Physical Sciences. 2011;6(36):8018-8026.

[6] Prakash J, et al. Effect of peristaltic flow of a third grade fluid in a tapered asymmetric channel. Journal of Physics: Conference Series. IOP Publishing, 2018;1000(1).

[7] Akbar NS, Hayat T, Nadeem S, Obaidat S. Peristaltic flow of a Tangent hyperbolic fluid in an inclined asymmetric channel with slip and heat transfer Progress in Computational Fluid Dynamics, an International Journal. 2012;12(5):363-374.

[8] Prabakaran PH, Kavitha A, Saravana R, Reddy RH, Sreenadh S. Peristaltic transport of a fourth grade fluid between porous walls with suction and injection, International Journal of Pure and Applied Mathematics. 2013;86(2):293-300.

[9] Eldabe NTM, Ahmed Y, Ghaly AY, Sallam SN, Elagamy K, Younis YM. Hall effect on peristaltic flow of third order fluid in a porous medium with heat and mass transfer, Journal of Applied Mathematics and Physics. 2015;3:1138-115.

[10] Abbas M Ali, et al. Three dimensional peristaltic flow of hyperbolic tangent fluid in non-uniform channel having flexible walls. Alexandria Engineering Journal. 2016;55(1):653-662.

[11] Saravana R, Hemadri Reddy R, Sreenadh S. MHD peristaltic flow of a hyperbolic tangent fluid in a non-uniform channel with heat and mass transfer, IOP Conference Series: Materials Science and Engineering. 2017;263(6):062006.

[12] Narasimhudu K Subba, Subba Reddy MV. Hall effects on the peristaltic pumping of a hyperbolic tangent fluid in a planar channel. Int. J. Math. Arch. 2017;8(3):70-85.

[13] Sucharitha G, et al. Effects of magnetic field and slip on convective peristaltic flow of a non-Newtonian fluid in an inclined nonuniform porous channel with flexible walls. Journal of porous media. 2018;21(10).

[14] Selvi CK, Srinivas ANS. Peristaltic transport of Herschel-Bulkley fluid in a non-uniform elastic tube. Propulsion and Power Research. 2019;8(3):253-262.

[15] Li A., et al. The use of an impulse magnetic field in the combined therapy of patients with stone fragments in the upper urinary tract. Voprosy Kurortologii, Fizioterapii, i Lechebnoi Fizicheskoi Kultury 1994;3:22-24.

[16] Devaki P, et al. Peristaltic flow of ferromagnetic fluid in a vertical slot with mixed convection. Recent Advances in Applied Mathematics and Applications to the Dynamics of Fluid Flows: 5th International Conference on Applications of Fluid Dynamics (ICAFD) 2020. Singapore: Springer Nature Singapore; 2022.

[17] Chakradhar K, et al. Investigation of peristaltic motion of viscous fluid in a porous channel with Suction and Injection by using Numerical technique.(Galerkin method). Specialusis Ugdymas. 2022;1(43):4214-4222.

[18] Vaidya Hanumesh, et al. Combined effects of chemical reaction and variable thermal conductivity on MHD peristaltic flow of Phan-Thien-Tanner liquid through inclined channel. Case Studies in Thermal Engineering. 2022;36:102214.

[19] Gangavathi P, et al. Slip and hall effects on the peristaltic flow of a Jeffrey fluid through a porous medium in an inclined channel. Materials Today: Proceedings. 2023;80:1970-1975.

[20] Ajithkumar M, Lakshminarayana P, Vajravelu K. Peristaltic transport of MHD Ree–Eyring fluid through a flexible channel under the influence of activation energy. Physics of Fluids. 2023;35(6).

Peer-review history:
The peer review history for this paper can be accessed here (Please copy paste the total link in your browser address bar)
https://www.sdiarticle5.com/review-history/105036